



Journal of Mechanical Science and Technology 32 (2) (2018) 793~798 www.springerlink.com/content/1738-494x(Print)/1976-3824(Online) DOI 10.1007/s12206-018-0127-z

Full-state-feedback, Fuzzy type I and Fuzzy type II control of MEMS accelerometer †

Ahmadreza Najafi and Jafar Keighobadi*

Department of Mechanical Engineering, University of Tabriz, Tabriz, Iran

(Manuscript Received March 29, 2017; Revised October 27, 2017; Accepted November 10, 2017)

Abstract

This paper presents classic and knowledge-based intelligent controllers for regulation of a vibratory MEMS accelerometer. The proposed methods comprise Fuzzy type I (FTI), Fuzzy type II (FTII) and Full-state-feedback (FSF) control systems. An ideal model of sensor under FSF controller is used to generate the required reference data to train if-then rule-base and Membership functions (MFs) of both fuzzy controllers. Through feeding the reference data as well as the FTI/FTII output into an Adaptive neural fuzzy inference system (ANFIS), the rules and MFs of the FTI/FTII system are updated. The control systems are realized by adding a Kalman filter (KF) loop to the force-balancing method for estimation of state variables and input acceleration. Stochastic noises are filtered out while keeping good tracking performance of MEMS accelerometer and reducing the displacement of the mass under the closed-loop ANFIS-KF structure.

Keywords: MEMS accelerometer; Fuzzy type II; Full state feedback; ANFIS; Force-balancing; Extended Kalman filter

1. Introduction

Owing to high performance, small size and greater functionality, MEMS accelerometers are used in industry [1]. The accelerometer consisting of a proof mass and an elastic beam is modeled as a mass-spring-damper system. By measuring the proof mass displacement relative to the sensor frame, an input acceleration is estimated by observing control forces. Energy dissipation by damping and measurement fluctuations guide to thermal-mechanical noises that decrease the sensitivity [2, 3]. To increase robustness against noise and disturbance, two force-balance [2] and compensator in the loop [4] methods are applied. A real-time force-balance method is applicable with analog output of sensor. However, controllers together with analog-to-digital converters show better results due to the high robustness of digital signals to noise [5]. Beyond robust methods as an alternative to sigma-delta approach [6, 7], Adaptive neural fuzzy inference system (ANFIS) is presented to improve the sensor performance by black box inferencing [8], while a Kalman filter (KF) is used to attenuate the noise of sensor and estimate the input values [9]. The predictive force-balancing control of a MEMS gyroscope was investigated without discussion about fuzzy methods [3]. A Fuzzy type I (FTI) control of a mobile robot by expert knowledge was introduced [10]. Now, following modelling of the MEMS accelerometer, we propose the Full-state-feedback

Using the ANFIS, the MFs and rules of both the FTII and FTI systems are constructed with respect to estimated displacement and velocity of the mass. Therefore, instead of try-and-error tuning of preceding fuzzy system as expert knowledge, the online ANFIS leads to accurate adaptive fuzzy controls. Unlike Refs. [11, 12], we designed the ANFIS with desired minimal parameters of MFs, while the rules number was independent of the input and output MFs. Therefore, the overall number of MFs and therein parameters to be updated in ANFIS are significantly decreased as well as the convergence rate of estimation is increased. Consequently, time-varying input accelerations can be estimated online by the proposed control system. Unlike the open loop reference model of sensor [10], we used an FSF control reference model to make the learning of ANFIS straightforward.

The configuration of the MEMS accelerometer includes a proof mass suspended by spring suspension and fixed electrodes in Fig. 1. The dissipation of mechanical energy caused

⁽FSF), and new FTI and Fuzzy type II (FTII) control methods. Using a KF, unavailable variables and parameters were estimated. Unlike to quasi-static function [3], we applied a complete dynamic of sensor in the framework of KF's state and parameter estimation, which allows measuring time-varying input acceleration rather than step inputs. Based on controllers of the sensor, the tracking and estimation performance against the measurement noises and structural uncertainty were assessed by simulations.

^{2.} Dynamics of MEMS accelerometer

^{*}Corresponding author. Tel.: +98 4133354153, Fax.: +98 4133393045

E-mail address: keighobadi@tabrizu.ac.ir

[†]Recommended by Associate Editor Dong-Weon Lee

[©] KSME & Springer 2018

by the structural damping and viscous effects of the ambient atmosphere, is considered by damping B along X -direction and the linear stiffness K. Regarding Newton's second law, the model of vibratory mass is obtained:

$$M\ddot{Q} + B\dot{Q} + KQ = MA_{ui} + U, \tag{1}$$

where M, A_{ui} and U stand for proof mass, acceleration and electrostatic control force, respectively. By introducing the reference mass, frequency, length and time as, M, ω^* , $q^* = (\omega^*)^{-2}$ and $t^* = t\omega^*$, non-dimensional Eq. (2) is obtained. Considering the thermal-mechanical noise w, measurement noise v_y , and parameters uncertainty as Δk and Δb , Eq. (2) is represented in the state space of Eq. (3) with \cdot^T being the transpose. The displacement Q is obtained by the coefficient h of the measured voltage v [9], with c being the capacitor capacity, ε_0 , ε_r the electric permittivity of vacuum and relative dielectric constant, d_0 is the distance between fixed plate and movable seismic mass when the mass is in the middle, a and v_1 are area of the plate and operation voltage, respectively.

$$\ddot{q} + b\dot{q} + kq = a_{ui} + u, \qquad (2)$$

$$q \to \frac{Q}{q^*}; b \to \frac{B}{M\omega^*} k \to \frac{K}{M\omega^{*2}} a_{ui} \to \frac{A_{ui}}{q^*\omega^{*2}} u \to \frac{U}{Mq^*\omega^{*2}},$$

$$\dot{x} = Ax + B(a_{ui} + u + w), \qquad (3)$$

$$y = v = Cx + v_y,$$

$$A = \begin{bmatrix} 0 & 1 \\ -(k + \Delta k) & -(b + \Delta b) \end{bmatrix} B = \begin{bmatrix} 0 \\ 1 \end{bmatrix} C = \begin{bmatrix} \frac{1}{q^*h} \\ 0 \end{bmatrix}$$

$$x = \begin{bmatrix} x_1 & x_2 \end{bmatrix}^T = \begin{bmatrix} q & \dot{q} \end{bmatrix}^T \cdot Q = hv = \frac{cd_0^2}{2\varepsilon_0 \varepsilon_r av_1} v.$$

3. State observer definition

Owing to a lack of access to all variables and uncertainty, the KF is set in output feedback loop to estimate displacement and velocity of proof mass and the acceleration [9]:

$$\begin{bmatrix} \dot{\hat{x}}_{1} \\ \dot{\hat{x}}_{2} \\ \dot{\hat{a}}_{ui} \end{bmatrix} = A_{a} \begin{bmatrix} \hat{x}_{1} \\ \hat{x}_{2} \\ \hat{a}_{ui} \end{bmatrix} + \begin{bmatrix} 0 \\ u \\ 0 \end{bmatrix} + L(t) \begin{bmatrix} y - C_{a} \begin{bmatrix} \hat{x}_{1} \\ \hat{x}_{2} \\ \hat{a}_{ui} \end{bmatrix} \end{bmatrix},$$

$$\dot{P} = A_{a}^{T} P + P A_{a} + P C_{a}^{T} R_{v}^{-1} C_{a} P + B_{a} R_{w} B_{a}^{T},$$

$$L(t) = P C_{a}^{T} R_{v}^{-1}.$$

$$A_{a} = \begin{bmatrix} 0 & 1 & 0 \\ -k & -b & 0 \\ 0 & 0 & -\beta \end{bmatrix} B_{a} = \begin{bmatrix} 0 \\ \Delta \\ \sqrt{2 \beta \sigma^{2}} \end{bmatrix} C_{a}^{T} = \begin{bmatrix} (q^{*} h)^{-1} \\ 0 \end{bmatrix}$$

$$(4)$$

where the KF gain L is obtained in terms of estimation co-

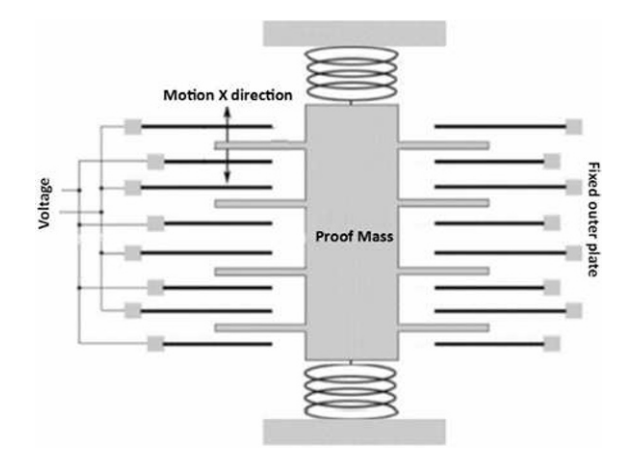


Fig. 1. Schematic of an x-axis MEMS vibratory accelerometer.

variance matrix P. R_v and R_w are covariances of v_y and w together with the distribution vector B_a of process noise and the gathered weight Δ of uncertainty and noises. β and σ^2 , respectively, denote the inverse of correlatin time and variance of Gauss-Markov model of input acceleration in KF.

4. Control strategy

Here, the force balancing method is designed to keep the mass displacement to zero by three FSF, FTI and FTII controllers. The schematic of the MEMS sensor together with the FTI and FTII controllers and the KF is shown in Fig. 2(a). The ANFIS structure in Fig. 2(b) is used to automatically produce the rules-base and MFs of both fuzzy systems. An FSF control is also imposed on model Eq. (3) without uncertainty and noises to generate desired control signal of ANFIS learning.

The classic FSF method is replaced to the fuzzy controller block of Fig. 2(a) without its learning section, Fig. 2(b). Since, the system Eq. (3) is controllable by Eq. (5), the Ackerman method is used to adjust feedback gains, k based on desirable characteristic equation, D(s) with sufficiently-large positive values $\alpha_1 \cdot \alpha_2$. Hence, the closed-loop stability of FSF is satisfied.

$$Rank\left(\left\lceil B \ AB \right\rceil\right) = 2,\tag{5}$$

$$D(s) = s^2 + \alpha_1 s + \alpha_2 \tag{6}$$

$$k = \lceil k_1 k_2 \rceil = \lceil 01 \rceil \lceil B \quad AB \rceil^{-1} D(A), \tag{7}$$

$$u(t) = -kx(t). (8)$$

4.1 FTI and FTII controllers

A type I fuzzy set, Z_i is characterized by a type-I MF as, $\mu_{Z_i}(r)$ where $0 \le \mu_{Z_i}(r) \le 1$ and $r \in R$ is the input argument. By blurring a type-I MF to left and to right, a type-2 MF is produced. Therefore, in a type-II MF, there exists an area between its lower and upper type-I MFs denoted by $\mu_{Z_i}(r)$ and $\overline{\mu}_{Z_i}(r)$, that is, more uncertainty is handled.

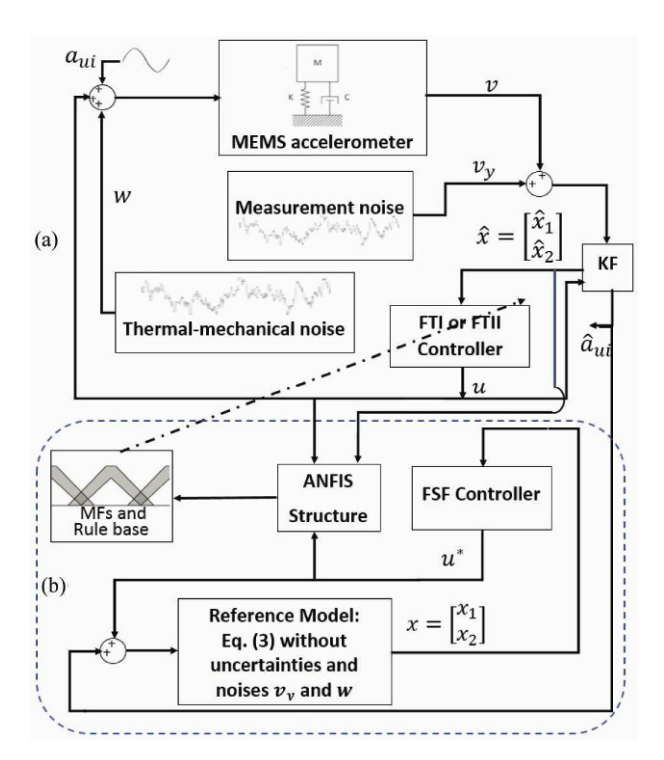


Fig. 2. MEMS accelerometer control: (a) FTI and FTII; (b) ANFIS.

Three fuzzy sets are considered for each of the estimated displacement and velocity by KF, so r will be \hat{x}_1 or \hat{x}_2 . The if-then rules of both FTI and FTII are as (i, j = 1:3):

FTI: IF \hat{x}_1 is μ_{d_i} AND \hat{x}_2 is μ_{v_j} THEN u is u_{ij} .

IF
$$\hat{x}_1$$
 is $\left\{\frac{\underline{\mu}_{d_i}}{\overline{\mu}_{d_i}}\right\}$ AND \hat{x}_2 is $\left\{\frac{\underline{\mu}_{v_j}}{\overline{\mu}_{v_j}}\right\}$ THEN u is $\left[u_{l_j}, u_{r_j}\right]$.

The subscripts d and v denote displacement and velocity. Using product T-norm, weighted average defuzzification and Type-Reducer of FTII guide to Non-fuzzy output [13]:

$$\mu_{ij}(\hat{x}_1.\hat{x}_2) = \mu_{d_i}(\hat{x}_1) \times \mu_{\nu_j}(\hat{x}_2),$$
(9)

$$u = \frac{\sum_{i=1}^{3} \sum_{j=1}^{3} \mu_{ij} (\hat{x}_{1}.\hat{x}_{2}) u_{ij}}{\sum_{i=1}^{3} \sum_{j=1}^{3} \mu_{ij} (\hat{x}_{1}.\hat{x}_{2})},$$
(10)

$$\mu_{ij}(\hat{x}_1.\hat{x}_2) = \mu_i(\hat{x}_1) \times \mu_{v_i}(\hat{x}_2), \tag{11}$$

$$\overline{\mu}_{ij}(\hat{x}_1.\hat{x}_2) = \overline{\mu}_{d_i}(\hat{x}_1) \times \overline{\mu}_{v_i}(\hat{x}_2), \tag{12}$$

$$u_{l} = \frac{\sum_{i=1}^{3} \sum_{j=l}^{3} \underline{\mu}_{ij} \left(\hat{x}_{1}.\hat{x}_{2}\right) u_{l_{ij}}}{\sum_{i=1}^{3} \sum_{j=l}^{3} \underline{\mu}_{ij} \left(\hat{x}_{1}.\hat{x}_{2}\right) u_{r_{ij}}}. u_{r} = \frac{\sum_{i=1}^{3} \sum_{j=l}^{3} \overline{\mu}_{ij} \left(\hat{x}_{1}.\hat{x}_{2}\right) u_{r_{ij}}}{\sum_{i=1}^{3} \sum_{j=l}^{3} \overline{\mu}_{ij} \left(\hat{x}_{1}.\hat{x}_{2}\right)}$$
(13)

$$u = \frac{u_l + u_r}{2},\tag{14}$$

with Eqs. (9) and (10) for FTI and Eqs. (11)-(14) for FTII using type-reducer defuzzification of Eqs. (13) and (14) [13].

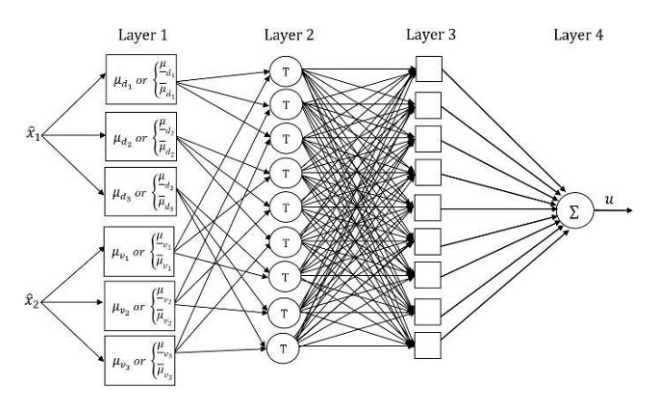


Fig. 3. Structure of ANFIS model.

The FTII damp the uncertainty by its interval membership grades. More adaptability, easier output-input relation in complex models and smooth control surface are the other advantages of FTII over FTI. More parameters to be updated by ANFIS and computational cost suffer the FTII.

5. ANFIS architecture

The ANFIS theory based on hybrid learning algorithm [11, 12], is proposed to create the entire parameters of MFs and ifthen rules of both fuzzy systems. In the illustrated four layers ANFIS architecture of Fig. 3, the square nodes as layer 1 refer to same Gaussian MFs. In layer 2, by circle nodes labeled T, the product T-norm of Eqs. (9), (11) and (12) is imposed on each single input from layer 1. The circles represent the firing strength of If-Then rules. In layer 3, triple Gaussian MFs, i.j = 1.3, are applied on estimated displacement and velocity as:

$$\mu_{d_i}(\hat{x}_1) = \exp\left(-\left(\frac{\hat{x}_1 - m_{d_i}}{\sigma_{d_i}\sqrt{2}}\right)^2\right),\tag{15}$$

$$\underline{\mu}_{d_i}(\hat{x}_1) = \rho_{d_i} \exp\left(-\left(\frac{\hat{x}_1 - \overline{m}_{d_i}}{\underline{\sigma}_{d_i}\sqrt{2}}\right)^2\right),\tag{16}$$

$$\overline{\mu}_{\nu_{j}}(\hat{x}_{2}) = \exp\left(-\left(\frac{\hat{x}_{2} - \overline{m}_{\nu_{j}}}{\overline{\sigma}_{\nu_{j}}\sqrt{2}}\right)^{2}\right),\tag{17}$$

where Eq. (15) is a FTI MF, and Eqs. (16) and (17) are FTII ones, e.g., $\overline{\mu}_{v_j}$ stands for upper MF of \hat{x}_2 ; to make lower MFs, $0 < \rho_{d_i} \cdot \rho_{v_i} < 1$ are multiplied to upper MFs.

In square nodes of layer 3, the left-right firing points of FTII in Eq. (13) are regarded. At layer 4, Σ yields aggregated output from the type-reducer of individual rules inference.

For online learning the ANFIS structure, the estimated displacement and velocity by KF and the reference control force, u^* generated by imposing the FSF controller on the reference model of Fig. 2(b) are used. Based on n numbers of data set p, the cost function of Eq. (18) including squared prediction errors of control force, e_p is minimized for ANFIS learning [11]. The force u_p is generated by FTI /FTII controller. Re-

ferring to Eq. (10), the singleton MFs of consequent part and the parameters of antecedent part of FTI rules are updated by gradient descent as, Eqs. (19)-(23) where, γ is a learning constant. As Eq. (13), the FTII is updated by Eqs. (24)-(33).

$$E = \frac{1}{2} \sum_{p=1}^{n} e_{p}^{2} \cdot e_{p} = u_{p}^{*} - u_{p}$$

$$u_{ij}^{new} = u_{ij}^{old} + \gamma e_{p} \frac{\mu_{ij} \left(\hat{x}_{1}.\hat{x}_{2}\right)}{\sum_{i=1}^{3} \sum_{j=i}^{3} \mu_{ij} \left(\hat{x}_{1}.\hat{x}_{2}\right)}$$

$$m_{d_{i}}^{new} = m_{d_{i}}^{old} + \gamma e_{p} \frac{\mu_{d_{i}} \left(\hat{x}_{1}\right) \left(\hat{x}_{1} - m_{d_{i}}\right) \sum_{j=1}^{3} \left(\mu_{v_{j}} \left(\hat{x}_{2}\right) \left(u_{ij} - u\right)\right)}{\left(\sigma_{d_{i}}\right)^{2} \sum_{i=1}^{3} \sum_{j=i}^{3} \mu_{ij} \left(\hat{x}_{1}.\hat{x}_{2}\right)}$$

$$m_{v_{j}}^{new} = m_{v_{j}}^{old} + \gamma e_{p} \frac{\mu_{v_{j}} \left(\hat{x}_{2}\right) \left(\hat{x}_{2} - m_{v_{j}}\right) \sum_{i=1}^{3} \left(\mu_{d_{i}} \left(\hat{x}_{1}\right) \left(u_{ij} - u\right)\right)}{\left(\sigma_{v_{j}}\right)^{2} \sum_{i=1}^{3} \sum_{j=i}^{3} \mu_{ij} \left(\hat{x}_{1}.\hat{x}_{2}\right)}$$

$$(20)$$

$$\sigma_{d_{i}}^{new} = \sigma_{d_{i}}^{old} + \gamma e_{p} \frac{\mu_{d_{i}}(\hat{x}_{1})(\hat{x}_{1} - m_{d_{i}})^{2} \sum_{j=1}^{3} (\mu_{v_{j}}(\hat{x}_{2})(u_{ij} - u))}{(\sigma_{d_{i}})^{3} \sum_{i=1}^{3} \sum_{j=1}^{3} \mu_{ij}(\hat{x}_{1}.\hat{x}_{2})}$$
(22)

$$\sigma_{v_{j}}^{new} = \sigma_{v_{j}}^{old} + \gamma e_{p} \frac{\mu_{v_{i}}(\hat{x}_{2})(\hat{x}_{2} - m_{v_{j}})^{2} \sum_{i=1}^{3} (\mu_{d_{i}}(\hat{x}_{1})(u_{ij} - u))}{(\sigma_{v_{j}})^{3} \sum_{i=1}^{3} \sum_{j=1}^{3} \mu_{ij}(\hat{x}_{1}.\hat{x}_{2})}$$
(23)

$$u_{l_{ij}}^{new} = u_{l_{ij}}^{old} + \gamma e_{p} \frac{\underline{\mu}_{ij} (\hat{x}_{1}.\hat{x}_{2})}{\sum_{i=1}^{3} \sum_{j=1}^{3} \underline{\mu}_{ij} (\hat{x}_{1}.\hat{x}_{2})}$$
(24)

$$u_{\eta_{j}}^{new} = u_{\eta_{j}}^{old} + \gamma e_{p} \frac{\overline{\mu}_{i}(\hat{x}_{1}.\hat{x}_{2})}{\sum_{i=1}^{3} \sum_{j=1}^{3} \overline{\mu}_{i}(\hat{x}_{1}.\hat{x}_{2})}$$
(25)

$$\overline{m}_{d_{i}}^{new} = \overline{m}_{d_{i}}^{old} + \frac{\gamma e_{p} \overline{\mu}_{d_{i}} \left(\hat{x}_{1}\right) \left(\hat{x}_{1} - \overline{m}_{d_{i}}\right) \sum_{j=1}^{3} \left(\overline{\mu}_{v_{j}} \left(\hat{x}_{2}\right) \left(u_{r_{j}} - u_{r}\right)\right)}{\left(\overline{\sigma}_{d_{i}}\right)^{2} \sum_{j=1}^{3} \overline{\lambda}_{j=1}^{3} \overline{\mu}_{j} \left(\hat{x}_{1}.\hat{x}_{2}\right)}$$

$$\overline{m}_{v_{j}}^{new} = \overline{m}_{v_{j}}^{old} + \frac{\gamma e_{p} \overline{\mu}_{v_{j}} (\hat{x}_{2}) (\hat{x}_{2} - \overline{m}_{v_{j}}) \sum_{i=1}^{3} (\overline{\mu}_{d_{i}} (\hat{x}_{1}) (u_{r_{ij}} - u_{r}))}{(\overline{\sigma}_{v_{j}})^{2} \sum_{i=1}^{3} \sum_{j=1}^{3} \overline{\mu}_{ij} (\hat{x}_{1}.\hat{x}_{2})}$$

$$\underline{\underline{\sigma}}_{d_{i}}^{new} = \underline{\underline{\sigma}}_{d_{i}}^{old} + \frac{\gamma e_{p} \underline{\mu}_{d_{i}} (\hat{x}_{1}) (\hat{x}_{1} - \underline{m}_{v_{j}})^{2} \sum_{j=1}^{3} (\underline{\mu}_{v_{j}} (\hat{x}_{2}) (\underline{u}_{l_{i_{j}}} - \underline{u}_{l}))}{(\underline{\sigma}_{d_{i}})^{3} \sum_{i=1}^{3} \sum_{j=1}^{3} \underline{\mu}_{i_{j}} (\hat{x}_{1} \cdot \hat{x}_{2})}$$

$$\underline{\sigma}_{v_{j}}^{new} = \underline{\sigma}_{v_{j}}^{old} + \frac{\gamma e_{p} \underline{\mu}_{v_{j}}(\hat{x}_{2})(\hat{x}_{2} - \underline{m}_{v_{j}})^{2} \sum_{i=1}^{3} (\underline{\mu}_{d_{i}}(\hat{x}_{1})(u_{t_{ij}} - u_{t}))}{(\underline{\sigma}_{v_{j}})^{3} \sum_{i=1}^{3} \sum_{j=1}^{3} \underline{\mu}_{ij}(\hat{x}_{1}.\hat{x}_{2})}$$
(28)

$$\overline{\sigma}_{d_{i}}^{new} = \overline{\sigma}_{d_{i}}^{old} + \frac{\gamma e_{p} \overline{\mu}_{d_{i}}(\hat{x}_{1})(\hat{x}_{1} - \overline{m}_{d_{i}})^{2} \sum_{j=1}^{3} (\overline{\mu}_{v_{j}}(\hat{x}_{2})(u_{r_{ij}} - u_{r}))}{(\overline{\sigma}_{d_{i}})^{3} \sum_{i=1}^{3} \sum_{j=1}^{3} \overline{\mu}_{ij}(\hat{x}_{1}.\hat{x}_{2})}$$
(30)

Table 1. Parameters of FTI controller.

Parameter	Value	Parameter	Value
u_{11}	8.5710 [μN]	m_{d_3}	0.04645
u_{12}	11.420 [μN]	$\sigma_{_{d_1}}$	0.02769
u_{13}	6.6410 [μN]	$\sigma_{\scriptscriptstyle d_2}$	0.02315
$u_{_{21}}$	1.3670 [μN]	$\sigma_{\scriptscriptstyle d_3}$	0.02689
u_{22}	0.1268 [μN]	$m_{_{ u_{_{1}}}}$	-0.007453
u_{23}	-1.5380 [μN]	m_{v_2}	0.00
$u_{_{31}}$	-6.7170 [μN]	m_{ν_3}	0.007543
$u_{_{32}}$	-11.5000 [μN]	$\sigma_{_{ u_{_{ m l}}}}$	0.003475
$u_{_{33}}$	-8.3890 [μN]	$\sigma_{_{v_2}}$	0.01153
m_{d_1}	-0.04646	$\sigma_{_{v_3}}$	0.003298
m_{d_2}	0.00	γ	0.2

$$\overline{\sigma}_{v_{j}}^{new} = \overline{\sigma}_{v_{j}}^{old} + \frac{\gamma e_{p} \overline{\mu}_{v_{j}} (\hat{x}_{2}) (\hat{x}_{2} - \overline{m}_{v_{j}})^{2} \sum_{i=1}^{3} (\overline{\mu}_{d_{i}} (\hat{x}_{1}) (u_{r_{ij}} - u_{r}))}{(\overline{\sigma}_{v_{j}})^{3} \sum_{i=1}^{3} \sum_{j=1}^{3} \overline{\mu}_{ij} (\hat{x}_{1} \cdot \hat{x}_{2})}$$

 $\rho_{d_{i}}^{new} = \rho_{d_{i}}^{old} + \frac{\gamma e_{p} \underline{\mu}_{d_{i}}(\hat{x}_{1}) \sum_{j=1}^{3} (\underline{\mu}_{v_{j}}(\hat{x}_{2})(u_{l_{ij}} - u_{l}))}{\sum_{j=1}^{3} \sum_{l=1}^{3} \mu_{l_{i}}(\hat{x}_{1}.\hat{x}_{2})}$ (32)

(31)

$$\rho_{v_{j}}^{new} = \rho_{v_{j}}^{old} + \frac{\gamma e_{p} \underline{\mu}_{v_{j}}(\hat{x}_{2}) \sum_{i=1}^{3} \left(\underline{\mu}_{d_{i}}(\hat{x}_{1}) \left(u_{l_{ij}} - u_{i} \right) \right)}{\sum_{i=1}^{3} \sum_{j=1}^{3} \mu_{ij}(\hat{x}_{1}, \hat{x}_{2})}.$$
 (33)

The final parameters trained by ANFIS in the FTI and FTII are listed in Tables 1 and 2.

6. Simulation results

First part of simulation in Simulink is done without uncertainty and noise, thereby in Eq. (3), w, v_v , Δk and Δb are considered zero. Next, to bring the simulated model closer to a real sensor, 15 % uncertainty of Δk and Δb as color noise and w, v_y as Gaussian white processes are applied to the plant. A sinusoidal acceleration a_{ui} with amplitude $1 g \text{ ms}^{-2}$ and a frequency of 50 Hz is applied to show the estimation capability of KF by dynamic model of sensor. The purpose is to estimate this input acceleration using the three controllers. The controller tries to fix the proof mass based on the forcebalance strategy. Owing to lack of a velocity sensor and affecting the sensor by noise as Eq. (3), the estimated displacement and velocity by KF are fed into the controllers. Also, the acceleration estimate is introduced as the Gauss Markov process in KF of Eq. (4). The effect of Δ is considered by 15 % increase of KF's process noise covariance and the plant parameters are listed in Table 3. The gains of FSF and the KF's covariance matrices, P(0), R_{u} and R_{u} are given by Table 3. For implementation of the FSF of Eq. (8) to MEMS plant, it

Table 2. Parameters of FTII controller.

Parameter	Value	Parameter	Value
$[u_{l_{i_1}}u_{r_{i_1}}]$	[8.321 8.821] [μN]	$\underline{\sigma}_{d_3}$	0.02693
$[u_{l_{12}}u_{r_{12}}]$	[11.09 11.75] [μN]	$ar{\sigma}_{\scriptscriptstyle d_1}$	0.02421
$[u_{l_{13}}u_{r_{13}}]$	[6.371 6.911] [μN]	$ar{\sigma}_{\scriptscriptstyle d_2}$	0.02245
$[u_{l_{21}}u_{r_{21}}]$	[1.257 1.477] [μN]	$ar{\sigma}_{\scriptscriptstyle d_3}$	0.02543
$[u_{l_{22}}u_{r_{22}}]$	[0.0968 0.1568] [μN]	$\underline{\sigma}_{v_1}$	0.0035
$[u_{l_{23}} u_{r_{23}}]$	[-1.768 -1.308] [μN]	$\underline{\sigma}_{v_2}$	0.01153
$[u_{l_{31}}u_{r_{31}}]$	[-7.154 -6.280] [μN]	$\underline{\sigma}_{v_3}$	0.0035
$[u_{l_{32}}u_{r_{32}}]$	[-12.014 -10.986] [μN]	$ar{\sigma}_{\scriptscriptstyle u_{_{\!\scriptscriptstyle 1}}}$	0.0032
$[u_{l_{33}}u_{r_{33}}]$	[-8.559 -8.219] [μN]	$ar{\sigma}_{_{ u_2}}$	0.01134
\overline{m}_{d_1}	-0.0455	$ar{\sigma}_{_{ u_{3}}}$	0.0032
\overline{m}_{d_2}	0.00	$ ho_{d_1}$	0.45
\overline{m}_{d_3}	0.04645	$ ho_{\scriptscriptstyle d_2}$	0.5
\overline{m}_{v_1}	-0.007453	$ ho_{\scriptscriptstyle d_3}$	0.45
\overline{m}_{v_2}	0.00	$ ho_{_{ u_{_{ m l}}}}$	0.54
\overline{m}_{v_3}	0.007543	$ ho_{v_2}$	0.48
$\underline{\sigma}_{d_1}$	0.02693	$ ho_{v_3}$	0.54
$\underline{\sigma}_{\scriptscriptstyle d_2}$	0.02315	γ	0.2

Table 3. Parameters of MEMS accelerometer, FSF controller and KF.

Parameter	Value	Parameter	Value
M	3.8e-9 kg	$v_{_1}$	0.6 volt
K	3 ±15% Nm ⁻¹	с	0.2e-10 F
В	0.7e-3 ±15% kgs ⁻¹	\mathcal{E}_r	4
а	1.86e-6 m ²	$d_{\scriptscriptstyle 0}$	2.3e-6 m
\mathcal{E}_0	8.85e-12 Fm ⁻¹	ω^*	20000 s ⁻¹
$R_{_{\scriptscriptstyle \mathcal{V}}}$	1e-4	g	9.81 ms ⁻²
$R_{_{\scriptscriptstyle W}}$	1e-4	$k_{\scriptscriptstyle 1}$	1.9737
P(0)	10I _{3×3}	k_2	9.2105

is replaced to the FTI/FTII controller block of Fig. 2(a). Compared with the FSF and FTI, FTII results in a better tracking performance and in the Fig. 4, the FSF imposes more control force on MEMS sensor. The statistical specifications of tracking and estimation errors in Table 4 show the close results of the FTII, FTI and FSF systems. From Table 4, without noise and uncertainty, the state tracking errors by FTII are superior with respect to those of the FTI and the FSF, while the input acceleration estimate of FSF is superior to the systems in the sense of standard deviation.

For perfect assessment of the controllers, a 15 % uncertainty is imposed by Δk and Δb parameters. Furthermore, the system is simultaneously affected by white noise of 0.001

Table 4. Errors Standard deviation (SD) without noise/uncertainty.

Controller	SD of displacement error [m]	SD of velocity error [ms ⁻¹]	SD of acceleration error [ms ⁻²]
FSF	0.0027	0.0008	0.2679
FTI	0.0017	0.0008	0.3500
FTII	0.0014	0.0011	0.3141

Table 5. SD of the errors under noise and uncertainty.

(Controller	SD of displacement error [m]	SD of velocity error [ms ⁻¹]	SD of acceleration error [ms ⁻²]
	FSF	0.0044	0.0009	0.5041
	FTI	0.0022	0.0008	0.4782
	FTII	0.0016	0.0007	0.3597
1	FTI / FTII	0.0047/0.0023	0.0066/0.0038	0.5562/0.3617

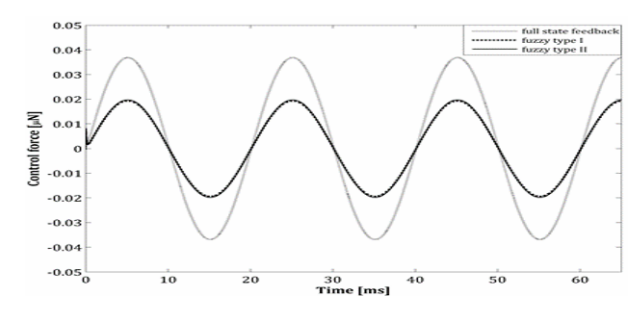


Fig. 4. Control force of FSF, FTI and FTII without noise/uncertainty.

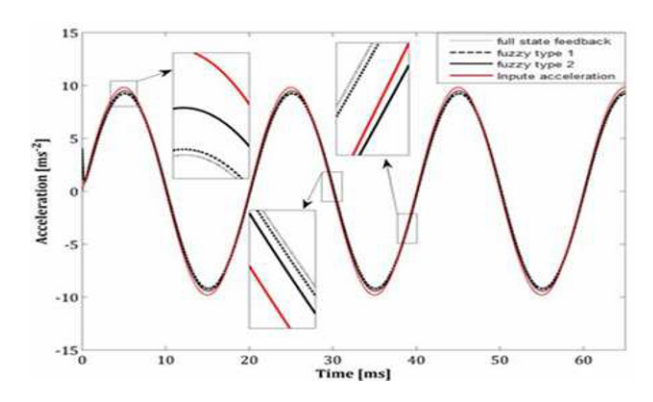


Fig. 5. Reference and estimated acceleration under noise/uncertainty.

SD and zero mean as measurement and thermal-mechanical noise of accelerometer. Comparison of Tables 4 and 5 shows that in the presence of noise and uncertainty, the state tracking error of the FSF controller is significantly increased. However, the tracking performance of fuzzy systems is more robust against noise and uncertainty. From Fig. 5 compared with the FSF, the fuzzy controllers, particularly type II, give a better tracking of reference accelerometer and displacement. The superiority of FTII system over the FTI and the FSF kinds is also detectable by remarkable decrease in the upper bound of tracking errors of reference accelerometer. Per Table 5, under noise the SDs of tracking errors by FTII decrease clearly with respect to those of the FTI and FSF controllers. The last row

of Table 5 provides a comparison between the performance of FTII and FTI in a situation where color noises of SD = 10^{-3} and mean = 0.005 for v_y , and SD = 10^{-2} and mean = 0.001 for w are imposed to the model. By $10{\sim}12$ % less tracking and estimation errors, the superiority of the FTII is vivid with respect to the FTI. Additionally, more improvements of both the FTII and FTI are accessible by increasing the number of MFs, which consequently increases the number of fuzzy rules and computational burden.

7. Conclusions

To keep the proof mass of vibratory MEMS accelerometer on desired zero velocity and displacement, three different control systems were proposed together with a KF's extended estimations of the displacement and velocity variables and the input acceleration. Beyond the FSF, the proposed novel FTI and FTII controllers in the force balancing loop were presented based on a new ANFIS with decreased number of parameters. Due to coincidence of the system model and controller without noise and uncertainty, the FSF system yielded perfect tracking and estimation accuracy as fuzzy controllers. However, the fuzziness structure of FTI and especially FTII systems resulted in robust and adaptive tracking performance in control of proof mass and in estimation of the unknown input acceleration. The FSF controller, owing to fixed proportional and differential gains, could not compensate for the uncertainties leading to large control force, and the estimation tracking errors unlike fuzzy controllers. The FTII controller showed better performance compared to the FTI kind, since the FTII structure includes greater adaptivity for uncertainty. Experimental validation of the results and development of 2axis MEMS accelerometer can be considered as future researches.

References

- [1] J. Lee et al., High-shock silicon accelerometer with an overrange stopper, *J. Mech. Sci. Technol.*, 30 (2016) 1817, https://doi.org/10.1007/s12206-016-0338-8.
- [2] J. Wu, Sensing and control electronics for low-mass low-capacitance MEMS accelerometer, Carnegie Institute of Technology (2002).
- [3] P. M. Hosseini and J. Keighobadi, Force-balancing model predictive control of MEMS vibratory gyroscope sensor, Proceedings of the Institution of Mechanical Engineers, Part C: J. of Mechanical Engineering Science, 230 (17) (2016) 3055-3065.
- [4] J. Keighobadi and M. J. Yarmohammadi, New chatter-free sliding mode synchronization of steer-by-wire systems under chaotic conditions, *J. of Mech. Sci. Technol.*, 30 (2016) 3829,

- https://doi.org/10.1007/s12206-016-0746-9.
- [5] K. L. Chau et al., An integrated force-balanced capacitive accelerometer for low-g applications, *Sensors and Actuators A: Physical*, 54 (1-3) (1996) 472-476.
- [6] C. H. Liu and T. W. Kenny, A high-precision, widebandwidth micromachined tunneling accelerometer, *J. of Microelectromechanical Systems*, 10 (3) (2001) 425-433.
- [7] E. Sarraf, B. Cousins, E. Cretu and S. Mirabbasi, Design and implementation of a novel sliding mode sensing architecture for capacitive MEMS accelerometers, *J. of Micromechanics and Microengineering*, 21 (11) (2011) 115033.
- [8] L. Zhang, J. Liu, J. Lai and Z. Xiong, Performance analysis of adaptive neuro fuzzy inference system control for MEMS navigation system, *Mathematical Problems in Engineering*, 2014 (2014) 1-7.
- [9] L. Dong and K. Zhang, Sensing and control of MEMS Accelerometers using KF, Control and Decision Conference (CCDC), 2012 24th Chinese: IEEE (2012) 3074-3079.
- [10] J. Keighobadi and M. B. Menhaj, From nonlinear to fuzzy approaches in trajectory tracking control of wheeled mobile robots, *Asian J. of Control*, 14 (4) (2012) 960-973.
- [11] J. R. Castro, O. Castillo, P. Melin and A. Rodríguez-Díaz, A hybrid learning algorithm for a class of interval type-2 fuzzy neural networks, *Information Sciences*, 179 (2009) 2175-2193.
- [12] J. Tavoosi, A. A. Suratgar and M. B. Menhaj, Stable ANFIS2 for nonlinear system identification, *Neurocomputing*, 182 (2016) 235-246.
- [13] O. Castillo, P. Melin, J. Kacprzyk and W. Pedrycz, Type-2 fuzzy logic: Theory and applications, *IEEE Granular Computing Conference*, Fremont, CA, USA (2007) 145-145.



Jafar Keighobadi received his Ph.D. in Control from Amirkabir University in Iran and joined the faculty of Mechanical Eng., Tabriz University in 2008. Dr. Keighobadi's research interests include applied nonlinear estimation/control.



thermal collectors.

Ahmadreza Najafi was born in Arak (Shazand), Iran, on Oct. 20, 1993. He received the B.S. degree in Mechanical Engineering from Department of Mechanical Engineering, University of Tabriz, (2012-2016). His research interests' areas are fuzzy systems, neural network, CFD modeling, and solar